RSC Advances

ROYAL SOCIETY OF CHEMISTRY

www.rsc.org/advances

Journal Name

RSCPublishing

ARTICLE

Morphological Evolution of Noble Metal Nanoparticles in Chloroform: Mechanism of Switching on/off by Protic Species

Cite this: DOI: 10.1039/xoxxoooooox

Received ooth January 2015,
Accepted ooth January 2015

DOI: 10.1039/xoxxoooooox

www.rsc.org/

O. A. Douglas-Gallardo [a], C. G. Gomez [b], M. A. Macchione [a], F. P. Cometto [a], E. A. Coronado [a], V. A. Macagno [a] and M. A. Pérez [a] *

The morphological stability/morphological reshaping of noble metal nanoparticles are studied experimentally in order to unravel the chemical mechanisms lying beneath. Gold and silver nanoparticles (AuNPs and AgNPs, respectively) formed in chloroformic environment are used, as model synthetic systems, to study phenomena of morphological change. The morphological evolution of NPs that follows their formation, is characterized by spectroscopy (UV-Visible, Raman and FTIR) and TEM (Transmission Electron Microscopy). The change of NP morphology involves the increase of the average NP size and the broadening of size distribution, in a close resemblance with the effect characteristically obtained from the Ostwald ripening. The effect of the poor solvating properties of chloroform in stabilizing small charged species (H^+, Ag^+, Au^+) as well as the principle of electroneutrality of matter are analyzed in order to formulate a feasible reaction scheme consisting of a three-step processes: the generation of soluble intermediary species by corrosion of nanoparticles, the diffusion of intermediary species from one nanoparticle to another, and the re-deposition process involving the reduction of intermediary species. This basic reaction scheme is used as hypothesis to plan and perform experiments, which reveal that molecular oxygen dissolved in the dispersive medium can drive NP corrosion, however, protic species are also required as co-reactant. The polarity of the hydrogen bond and the ligand properties of the anions produced by de-protonation are feature of the protic species that enable/disable the corrosion and, in turn, the NP morphological evolution.

Introduction

Crystals with at least one dimension within 1-100 nm exhibit electronic confinement conditions which differ from those found for molecules/atoms and extended solids. As a consequence, their chemical and physical properties are sui generis and depend on their size and shape[1-3]. In this size range, metallic particles are objects of interest from basic research viewpoint as well as from their applications[4-6]. Therefore, to attain control over NPs' size/shape is a crucial capability in developing basic and applied scientific research, which makes synthesis investigation a very active and dynamic field[4-18]. Synthetic methods of colloidal chemistry are among those more widely investigated[7] due to their high yield, low cost materials, and easy implementation. However, reproducibility and control of shape/size are aspects which demand for improvements yet.

About this last issue, we believe that the key for success in controlling morphological features is to understand the chemistry which governs formation and stability of NPs. This fundamental knowledge is not always accessible, mainly due to the complexity of synthetic systems frequently makes fuzzy the connection between morphological features and experimental factors (concentration and nature of reactive species, procedures, activation conditions, etc.). In this regard, the use of synthetic systems where selected experimental features were oversimplified (referred hereafter as "model synthetic systems") offers better possibilities for understanding the chemistry that controls formation and stability of NPs.

Once formed, nanoparticles can exhibit "stability" depending on the extension of the influence of different phenomena. Among them, Ostwald ripening is a main one and, consequently, its study becomes central for achieving control on nanoparticle morphology. Although Ostwald ripening is a phenomenon profusely cited within the literature, the approach to the problem is mainly addressed phenomenologically and, then the study of chemical mechanisms underlying this phenomenon can only be found in a handful of articles[19-21].

The present work is aimed at studying the chemical mechanisms underlying the phenomena of morphological stability/morphological reshaping of metallic nanoparticles. Model synthetic systems, based on in carrying out redox reactions with well-defined reactive species (such as $AuBr_4^-$, $Ag(SCN)_2^-$, Ag_2O and BH_4^-) in chloroform at room-temperature, are used to study the morphological stability of noble metal nanoparticles. Firstly, the spectroscopic and TEM evidence corresponding to the straightforward formation of NPs and their subsequent morphological evolution in chlroloformic medium is presented and discussed. Then a consistent reaction scheme is proposed, discussed and used as start hypothesis to perform conclusive experiments to reveal the main features of the chemical mechanism underlying the morphological evolution and stability.

Materials and Methods

Experimental

All stock solutions were prepared from analytical reagent chemicals as received and, according to the purpose, by using as solvent either purified water (Milli Ro-Milli Q system) or chloroform. Aqueous solutions containing silver nitrate ($AgNO_3$) and tetrachloroauric acid ($HAuCl_4$) were kept in darkness to prevent any photochemical reaction involving Ag(I) and Au(III) species.

Model synthetic systems based on redox reactions carried out in chloroform own several interesting features. Formation and growth of nanoparticles by using redox reactions can be driven out at room temperature within easy and safe procedures. Additionally, the use of non-aqueous dispersive media offers an alternative for studying synthetic systems under conditions in which some contributions to the Gibbs free energy change are different from those found for water, viz., solubility, dielectric constant, solvation of charged species, and diffusion. Regarding this last property for instance, it is clear that the Grotthuss mechanism which explain the high mobility of proton ions in water[22-23] can be disabled or disfavoured for protic species when non-protic solvents are used. Chloroform, because of its very low miscibility with water is an excellence candidate to be used as second liquid phase to perform extraction of aqueous complex species. In addition, the trimetyl-hexadecyl-ammonium bromide (CTAB) used as extraction agent is inexpensive and highly soluble in chloroform.

Synthesis of Precursors and Reducing Agent

Chloroformic solutions of precursor and reducing agents were obtained from extraction procedures, namely: aqueous | chloroform extraction[8,16,24-26] and solid | chloroform extraction (leaching)[27], respectively. The extractive solutions were prepared typically by dissolving CTAB in chloroform to be used as an extraction agent. Trimetyl-hexadecyl-ammonium nitrate (CTAN) was also used to extract particularly the silver coordination complex anions, given that the use of CTAB leads to AgBr precipitation. All chloroformic solutions obtained from extraction processes, hereafter are referred to as "liquors", were characterized by UV-Visible, IR, and Raman spectroscopy. With a procedure similar to those reported elsewhere[8,16], 50 mL of chloroformic solution containing 1 mM of the extraction agent (CTAB or CTAN) was mixed with 50 mL of an aqueous solution containing the anionic complex ($AuBr_4^-$ or $Ag(SCN)_2^-$) in a concentration of 2 mM. The resulting aqueous/chloroformic emulsion was shaken during 15 minutes and both phases were separated after being at rest for one hour in a separating funnel. The resulting chloroformic liquors were separated and dried with $CaCl_2$ to reduce any water content, and lately, stored in a closed vessel at 2 °C. It is important to stress that CTAB concentration values used to prepare the liquors (of precursor and reducing agents) fall down under 6 mM, value at which pre-micellar structures were reported for CTAB aqueous solution (CMC_{CTAB} = 40 mM)[23]. Thus, while pre-micellar / micellar supra molecular structures result appropriate to be regarded when biphasic synthetic systems are studied[8,10-13], they are not considered as relevant factor in analyzing the phenomena observed inside the homogeneous chloroformic medium given that the chloroformic liquors contain water only in very small amounts after the drying step.

Chloroformic solutions containing BH_4^-, bound to be used as reducing liquor, were prepared from the leaching of powdered solid $NaBH_4$ with a 10 mM CTAB chloroformic solution. Solid sodium borohydride ($NaBH_4$) was ground in a mortar into a fine powder, which was mixed with 50 mL of 10 mM CTAB chloroformic solution for leaching. The content of powdered $NaBH_4$ was set to be 10 times the CTAB mole amount contained in the leaching solution volume[27]. The mixture was kept under stirring during one day in a closed vessel at room-temperature to ensure the extraction process. After this leaching time, the liquor was filtered, dried with $CaCl_2$, and stored in a closed vessel at 2 °C.

Reducing and precursor agents obtained as liquors were characterized by UV-Visible, IR and Raman spectroscopy. A consistent analysis of spectroscopic results shows that chloroformic liquors containing $AuBr_4^-$, $[Ag(SCN)_2]^-$, and BH_4^- as counter anions of trimetyl-hexadecyl-ammonium are effectively produced from aqueous | chloroform and solid | chloroform extraction processes. The extracted liquor containing $AuBr_4^-$ is easily identified by its characteristic orange color (UV-Visible range, peaks at 260 nm and 394 nm)[29] as well as by Raman spectroscopy (109 cm^{-1}, 197 cm^{-1} and 212 cm^{-1})[30,31] . No colored $Ag(SCN)_2^-$ and BH_4^- were both identified by Raman and FTIR spectroscopy. Effective synthesis of $[CTA^+\cdots Ag(SCN)_2^-]$ was corroborated from the detection of -SCN asymmetric stretching band at 2109.34 cm^{-1} (Raman)[30,32] and at 2118 cm^{-1} (FTIR). The effective synthesis of $[CTA^+\cdots BH_4^-]$ was corroborated, in similar way, by the detection of FTIR absorption bands at 1126 cm^{-1}, 2225 cm^{-1} and 2293 cm^{-1} which are respectively associated with the antisymmetric bending, the antisymmetric stretching and symmetric stretching of BH_4^- [27,30,33]. The detection of a broad Raman signal at 2266 cm^{-1}, associated with both[27,30,33] symmetric and antisymmetric stretching of BH_4^-, provides additional support to the effectiveness of the leaching procedure.

Synthesis of NPs

In a typical experiment, liquors containing precursor agents and the reducing agent were mixed at room temperature and kept under constant stirring. In this procedure, a volume of the chloroformic liquor containing 10 mM ($CTA^+\cdots BH_4^-$) (V_r) is added dropwise into a volume of a 0.1 mM chloroform solution of either ($CTA^+\cdots Ag(SCN)_2^-$) or ($CTA^+\cdots AuBr_4^-$) (V_p) to obtain final volume ($V_f = V_r + V_p$) of a reactive solution. In this chloroformic reactive solution, reducing agent and precursor agents are in concentration values near to 1 mM and 0.1 mM, respectively. Final volume values (V_f) were typically larger than 5 mL to assure controllable convection conditions.

Characterization

IR and Raman samples were prepared by seeding many drops of chloroformic liquors / solutions on a compressed KBr pellet or on a glass slide, respectively; and letting chloroform evaporation to take place at room temperature. Non-volatile compounds contained in the liquors undergo re-precipitation to produce thin layer deposits, which were analyzed by IR and Raman spectroscopy. FTIR spectra were recorded on a Nicolet 5-SXC spectrometer by using a forty scan average and a resolution of 4 cm^{-1}. Raman spectra were recorded on a Horiba Jobin Yvon LabRAM HR Raman spectrometer by using a red laser (632.82 nm) as excitement source. UV-Visible spectra were recorded on a Shimadzu UV-1601 spectrometer by using a 1 cm quartz cell at room temperature to characterize the optical properties of species contained in liquors and the surface plasmon resonance (SPR) of gold (AuNPs) and silver (AgNPs) nanoparticles in chloroform.

Selected experimental samples of AuNPs and AgNPs produced with redox reactions in chloroform were characterized by TEM (JEM-JEOL 1120 microscope). Samples were prepared by using chloroformic solutions containing noble metal NPs without any purification treatment to seed one or two drops of solution onto a carbon-Formvar-covered cooper grid and by allowing for the evaporation of chloroform to occur at room temperature.

Statistical Analysis

Size distribution of NPs was determined by performing a digital analysis of TEM images. In order to calculate the frequency of each size value, the shape of NPs was a key feature to consider. Whereas spherical or nearly-spherical NPs are well characterized by their diameter, the largest longitudinal dimension of NPs with non-spherical shapes was chosen as the main parameter to consider. Such a criterion provides a simple and appropriate parameter to analyze the changes of average size and size distribution associated with the morphological evolution. NPs size population was described either by using a gaussian distribution, centered at $\langle d \rangle$ (average diameter) and with a dispersion of σ (variance rootsquare), or by indicating maximum frequency size (d_{mf}) and the lowest and highest values of NP size in the population (d_l, d_h).

Results and discussion

NPs formation and morphological evolution

In a typical experiment, the formation of NPs is carried out by adding dropwise, at room temperature, the reducing agent ($CTA^+\cdots BH_4^-$) solution into the liquors containing the precursor agent ($CTA^+\cdots Ag(SCN)_2^-$ or $CTA^+\cdots AuBr_4^-$). After five minutes of reaction, the products were characterized by UV-Visible spectroscopy and TEM. The reactive solution obtained in each case owns colors different from those corresponding to the initial precursor agent liquors. The reactive solution obtained in each case owns colors different from those corresponding to the initial precursor agent liquors. Thus, the change from the initially transparent $[CTA^+\cdots Ag(SCN)_2^-]$ - liquor to the final yellow solution after addition of $[CTA^+\cdots BH_4^-]$ - liquor is characteristic of the formation of AgNPs (ESI-Fig. 1). Similarly, after the addition of $[CTA^+\cdots BH_4^-]$ - liquor; the initially orange $[CTA^+\cdots AuBr_4^-]$ - liquor changes into a ruby-red solution, a color that is indicative of the AuNP formation (ESI-Fig. 1). In both cases, the extinction peaks observed for the blue line profiles at 416 nm in Fig. 1a and at 524 nm in Fig. 2a are associated with SPR bands of AgNPs and AuNPs formed in each case (Fig. 1c and Fig. 2c). The analysis of TEM micrographs indicates that the AgNP population is centered at $\langle d \rangle = 4.81$ nm and dispersed in $\sigma = 1.58$ nm (Fig. 1b, blue bars) whereas the AuNP population is centered at $\langle d \rangle = 6.1$ nm with a dispersion of $\sigma = 0.2$ nm (Fig. 2b, blue bars).

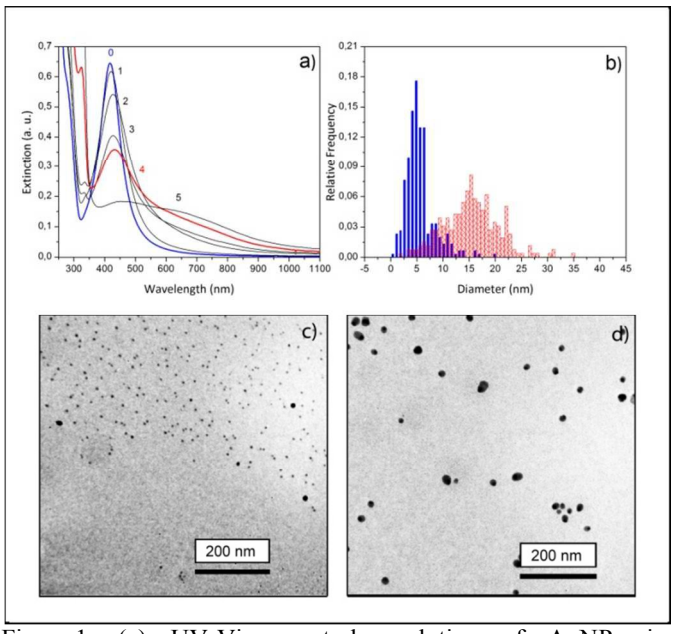

Figure 1. (a) UV-Vis spectral evolution of AgNPs in chloroform: (—) 5 min., (—) 1, (—) 2, (—) 3, (—) 4, and (—) 5 days. (b) Size distribution of AgNPs: (—) 5 min. after their formation ($\langle d \rangle = 4.81$ nm, $\sigma = 1.58$ nm) and (—) at the 4th day of evolution ($\langle d \rangle = 15.3$ nm, $\sigma = 4.93$ nm). (c) TEM images of AgNPs produced from the reduction of $[CTA^+\cdots Ag(SCN)_2^-]$ against $[CTA^+\cdots BH_4^-]$ immediately after their formation ($\langle d \rangle = 4.81$ nm, $\sigma = 1.58$ nm), and (d) after four days of evolution ($\langle d \rangle = 15.3$ nm, $\sigma = 4.93$ nm).

These chemical changes associated with the NPs formation in chloroform can be described according to:

$$2\left[CTA^+\cdots Ag(SCN)_2^-\right] + \left[CTA^+\cdots BH_4^-\right] \rightarrow \ldots$$
$$\ldots \rightarrow 2\,Ag_{(NP)} + BH_3 + HSCN + 3\left[CTA^+\cdots SCN^-\right] \quad (1)$$

and

$$2\left[CTA^+\cdots AuBr_4^-\right] + 3\left[CTA^+\cdots BH_4^-\right] \rightarrow \ldots$$
$$\ldots \rightarrow 2\,Au_{(NP)} + 3\,BH_3 + 3\,HBr + 5\left[CTA^+\cdots Br^-\right] \quad (2)$$

where the subscript (NP) stands for noble metal atoms aggregated as nanoparticles. The overall reactions are written in terms of neutral species since the formation of proton (H^+) from the oxidation of BH_4^- is considered improbable because of the poor solvation effect of chloroform for the stabilization of small ions. At difference of water which works as a source of oxide anions (O^{2-}) for rising up the oxidation state of reducing species; chloroform limits the oxidation reaction and BH_4^- cannot be oxidized further than BH_3.

After their formation, AgNPs and AuNPs in chloroformic media are colloids which stay perfectly stabilized as dispersed systems, given no evidence of agglomeration or decantation was detected. However, a gradual spectral evolution can be

noticed as time elapses. Fig. 1a exhibits the spectral evolution followed along five days, where the spectral profiles corresponding to freshly formed AgNPs (blue line) and to the colloidal suspension aged during four days (red line) are highlighted. The four-day aged colloidal suspension (Fig. 1a, red line) exhibits an extinction profile where the main SPR peak is shifted 36 nm to longer wavelength values when compared to that corresponding to freshly formed AgNPs. The whole profile is noticeably broaden, and a shoulder can be also observed at 770 nm. The analysis of TEM micrographs corresponding to the freshly formed and four-day aged suspensions (Fig. 1c and 1d, respectively) indicates that the spectral evolution takes place simultaneously with noticeable morphological changes. After four days of evolution, the average AgNPs' size (⟨d⟩) increases from 4.81 nm to 15.3 nm whereas the size distribution (σ) broadens from 1.58 nm to 4.93 nm (Fig. 1b).

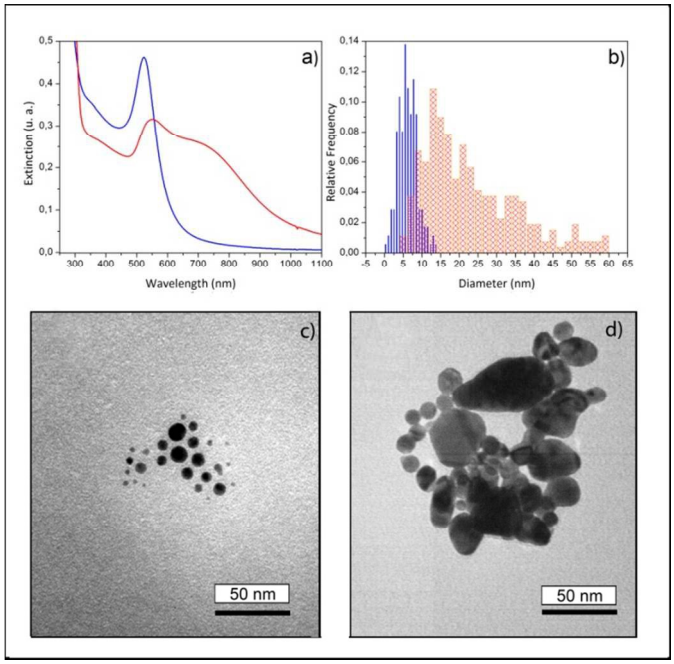

Figure 2. (a) UV-Vis spectral evolution of AuNPs in chloroform: (—) 5 min. after formation and (—) at the 5th day of evolution. (b) Size distribution of AuNPs: (—) 5 min. after their formation (⟨d⟩ = 6.1 nm, σ = 2.44 nm) and (—) at the 5th day of evolution (with d_{mf} = 15.9 nm, d_l = 4 nm and d_h = 60 nm). (c) TEM images of AuNPs produced with the reduction of [$CTA^+\cdots AuBr_4^-$] with [$CTA^+\cdots BH_4^-$] immediately after their formation (⟨d⟩ = 6.1 nm, σ = 2.47 nm.) and (d) after five days of evolution (d_{mf} = 15.9 nm and 4 nm < d < 60 nm).

Quite similar results were also obtained for AuNPs. After five days of evolution, AuNP chloroformic suspension exhibits a spectrum different from that corresponding to freshly prepared AuNPs, which shows a sharp SPR peak at 524 nm (Fig. 2.a, blue line). This evolved spectral profile is noticeably broader (Fig. 2a, red line) than that of freshly prepared AuNPs, with a main SPR peak at 560 nm and a shoulder at 770 nm. From the analysis of TEM micrographs at each stage (Fig. 2c, 2d), it can be observed that spectral evolution occurs with important morphological changes. After five days of evolution, the initial gaussian-type size distribution, centered at ⟨d⟩ = 6.1 nm with a dispersion of σ = 2.44 nm, is changed into a very broad size distribution with d ranging from 4 nm to 60 nm and d_{mf} = 15.9 nm (Fig. 2b). It is also worthy of noticing that observation of small size NPs (d < 4 nm) becomes infrequent after this evolution period, supporting the fact that size values increase in general terms without the formation of new small AuNPs.

Mechanism of morphological evolution

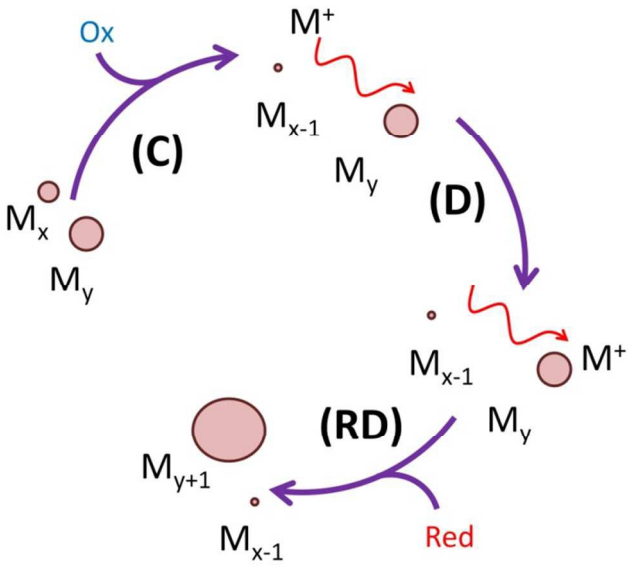

Scheme 1. The three-step sequence of corrosion (**C**), diffusion (**D**) and re-deposition (**RD**), where Ox and Red stand for the oxidizing and reducing species and, for the sake of simplicity, the soluble intermediary species are represented by M^+. Subscripts stand for the number of metallic atoms (**M**) in each NP.

It is important to remark that since no agglomeration nor decantation was detected during the evolution of the samples, the NPs suspensions were perfectly stable as disperse material systems. This clearly means that the change of size/shape of AgNPs and AuNPs takes place whereas NPs stay as a stabilized dispersed phase in the chloroformic medium. Re-shaping/re-sizing of NPs might involve then soluble intermediary species diffusing from one nanoparticle to another. Non-charged species like atoms can be considered as soluble intermediary species in a solvent like chloroform, however, in producing them from NPs requires activation energy values around the chemical bonds breakdown. The range from 155 to 215 kJ mol^{-1}, where chemical bond dissociation energies of Ag_2 / Au_2 fall down, allows a crude estimation of activation energy values to be made. Then, the activation energy needed for producing atoms from NPs is many times greater than the thermal activation (2.5 kJ mol^{-1}) available from the medium surrounding NPs. Thus, a mechanism involving atoms as soluble intermediary species seems rather unlikely. Instead, the dynamics of the morphological evolution of these stable colloidal systems might be described in terms of electrochemical processes. This phenomenon can be reasonably described by assuming a mechanism which involves the following three-step sequence: corrosion (**C**), diffusion (**D**) and re-deposition (**RD**) (Scheme 1). During the corrosion step (**C**), the NPs oxidation re-generates soluble oxidized species, which are complex anions of Ag(I) and Au(I)/Au(III) play the role of the soluble intermediary species. The second step

involves the diffusion of these soluble intermediary species from one NP to another (**D**). The final step of re-deposition (**RD**) is produced by the reduction of soluble intermediary species onto the surface of NPs.

Like any other colloidal system, NPs dispersed in chloroform can undergo Ostwald ripening due to their very high surface to volume ratio. The excess of surface Gibbs free energy (ΔG_s) of the colloidal system as compared to that of an equivalent bulk system is the driving force of the Ostwald ripening, whose overall effect is that large NPs increase their size at the expense of the dissolution of small ones. Ostwald ripening of colloids formed by ionic compounds in polar solvents or by weakly bonded molecular clusters where dissolution of particles requires small values of activation energy can be described appropriately by regarding the excess of surface Gibbs free energy (ΔG_s) as the leading term of the driving force. However, the driving force for the Ostwald ripening of AgNPs/AuNPs in chlorformic medium must include additional Gibbs free energy contributions coming from the redox reactions within **C** and **RD** steps. Thus, the actual driving force for the morphological evolution of AgNPs/AuNPs has a contribution coming from the excess of surface Gibbs free energy (ΔG_s), characteristic of all colloidal system, and an additional term accounting the Gibbs free energy coming from the contribution of chemical reactions within **C** and **RD** steps (ΔG_{chem}). Accordingly, the morphological evolution of AgNPs/AuNPs in chlorformic medium should be more appropriately termed as a *pseudo*-Ostwald ripening.

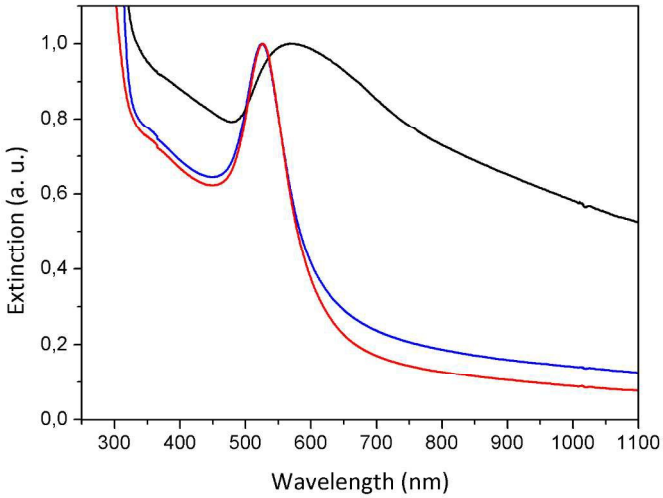

Figure 3. Normalized UV-visible spectra corresponding to AuNPs colloids aged during 15 days under O_2 concentration values achieved by: (—) saturation at the atmospheric O_2 pressure, and (—) after bubbling and storing the sample under a N_2 atmosphere. Reference: (—) freshly prepared chloroformic colloid of AuNPs.

In order to identify the oxidizing agent in the dispersion medium, a freshly prepared chloroformic colloid of AuNPs was brought to be aged in environments containing molecular oxygen concentration of different values. A first aliquot of suspension was left to evolve during fifteen days into a chloroformic medium saturated with molecular oxygen (at 20-25ºC). A second aliquot was profusely bubbled with nitrogen gas to reduce the content of molecular oxygen, sealed and left to evolve over the same aging period. After this aging time, the spectral profiles obtained for each aliquot are drastically different (Fig. 3). In a dispersive medium with high O_2 content, the aging of AuNPs leads to a spectral profile (Fig. 3, black line) noticeably different from that observed for the reference corresponding to freshly prepared colloid of AuNPs (Fig. 3, blue line). Located at longer wavelength values (c.a. 600 nm) than that of the reference (c.a. 520 nm), the main SPR peak is wide and followed by a slowly decreasing extinction tail as the wavelength increases. Theses spectral changes are associated with the morphological change that involves mainly the increase of size as in the case previously discussed (Fig. 2). The aging of AuNPs in a medium with low O_2 content leads to a spectral profile (Fig. 3, red line) very similar to that of the reference (Fig. 3, blue line). In this case, the main SPR peak shows no appreciable change of neither its wavelength position or its FWHM, features which strongly indicate that the initial population of AuNPs in the colloid did not suffer noticeable changes during the aging. This whole evidence leads to conclude that the molecular oxygen (O_2) can play the role of the oxidizing species needed to drive the corrosion step (**C**). This is in agreement with a previous work where molecular oxygen (O_2) is proposed as feasible oxidizing agent in organic media[34]. Anions SCN^- and Br^-, obtained as byproducts of the AgNPs/AuNPs formation reactions (1) and (2), do help the oxidizing action of O_2 within the formation of complexes with the oxidized species (Ag^+, Au^+, Au^{3+})[35-38] . It is evident that after NP formation, the experimental conditions are appropriate for the corrosion step (**C**) to produce soluble intermediary species.

A brief analysis of the experimental conditions of a typical experiment of synthesis helps to realize that leftover of the reducing agent (BH_4^-) remains from the formation of AgNPs/AuNPs. An excess of the reducing agent is regularly used in order to drive fast nucleation and growth and, consequently, BH_4^- is generally more concentrated than the particular precursor used ($AuBr_4^-$ or $Ag(SCN)_2^-$). Thus, these leftover quantities of BH_4^- can help in reducing the soluble intermediary species during the re-deposition (step **RD**).

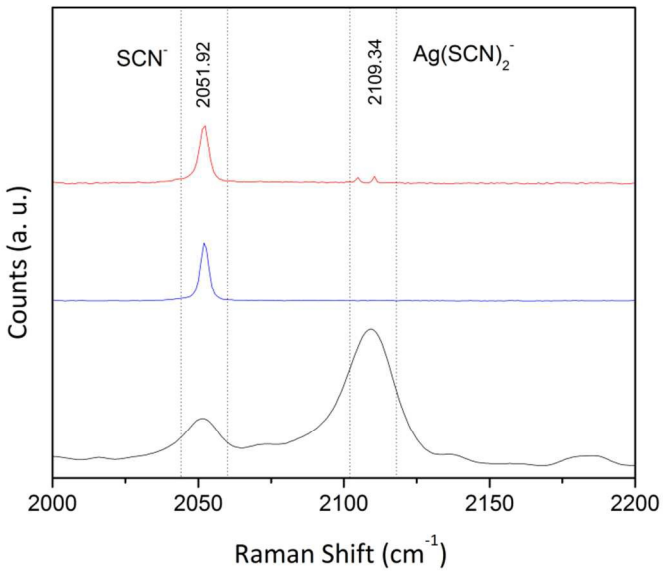

Figure 4. Raman spectra for: $[CTA^+\cdots Ag(SCN)_2^-]$ precursor (—), the reactive solution immediately after the addition of the reducing agent (—) and after four days of evolution (—). Intensity spectra is normalized by the intensity of the $[CTA^+\cdots SCN^-]$-signal at 2052.34 cm^{-1}.

For the sake of simplicity, the analysis of the soluble intermediary species will be focused on the case of silver nanoparticles; where the assumption that corrosion produces $Ag(SCN)_2^-$ can be experimentally explored. Raman spectroscopy was used as monitoring technique during the AgNP formation and subsequent morphological evolution (Fig. 4). In the region from

2000 cm^{-1} to 2200 cm^{-1}, the $[CTA^+\cdots Ag(SCN)_2^-]$ - liquor exhibits a Raman spectrum (Fig. 4, black line) with a strong signal at 2109.34 cm^{-1} associated with the asy mmetric stretching of $Ag(SCN)_2^-$. A second less intense signal at 2051.92 cm^{-1} corresponding to the asymmetric stretching of free SCN^- is also detected. This additional signal is frequently observed given that free SCN^- is also present in the liquor as a by-product co-extracted simultaneously with the silver precursor ($Ag(SCN)_2^-$). The addition of $[CTA^+\cdots BH_4^-]$, which drives the AgNP formation according to eq. (1), leads to a drastic decrease of $[CTA^+\cdots Ag(SCN)_2^-]$ concentration. This is plenty corroborated by the Raman spectrum obtained immediately after the addition of the reducing agent, where the signal associated with $Ag(SCN)_2^-$ is absent whereas the signal of free SCN^- became more intense (Fig. 4, blue line). Interestingly, the Raman spectrum recorded at the fourth day of morphological evolution exhibits a couple of signals in the region where the characteristic signal of $Ag(SCN)_2^-$ is typically observed. This evidence is clearly indicating the presence of $Ag(SCN)_2^-$, re-generated by the corrosion of small AgNP. These results also allow in establishing two different regimes: the NP formation and the pseudo-Ostwald ripening stages. During the formation stage, nucleation and growth of AgNPs take place inside a medium where $Ag(SCN)_2^-$ and BH_4^- are both in high concentration.

Towards the end of this stage, the concentration of $Ag(SCN)_2^-$ decreases to reach values drastically lower than those at the beginning of reaction. This stage leads to a population of AgNPs with an initial shape/size distribution inside a dispersive medium whose composition is mainly described by the right side of eq. (1) and important amounts of BH_4^- leftover. During the *pseudo*-Ostwald ripening stage, the small AgNP corrosion process driven by O_2 in presence of SCN^- re-generates $Ag(SCN)_2^-$ (**C** step), rising up its concentration to level values high enough to be detected by Raman spectroscopy. Under such conditions, $Ag(SCN)_2^-$ plays the role of soluble intermediary species which diffuses from one AgNP to another (**D** step). In this dispersive medium still rich in BH_4^-, the soluble intermediary species reacts on the surface of large AgNPs to give their size increase or change of shape (**RD** step). The continuous repetition of this key sequence of steps **C-D-RD** should generate through time cumulative changes within the initial shape/size distribution. Concentration of $Ag(SCN)_2^-$ during this stage is kept stationary at levels values which depends on the overall result between the generation rate by a "source process" (step **C**) and the consumption rate by a "drain process" (steps **RD**). In summary, the stage of formation can be clearly distinguished from the stage of *pseudo*-Ostwald ripening because the processes involved are different in each case (nucleation/growth and corrosion/diffusion/re-deposition, respectively). Moreover, both stages take place in media with different experimental composition: formation occurs into an environment rich in $Ag(SCN)_2^-$ whose concentration is constantly decreasing; whereas *pseudo*-Ostwald ripening takes place in a medium where the concentration of $Ag(SCN)_2^-$ has very low level and remains stationary.

Role of protic species

Even though this general scenario appears as enough detailed in describing the morphological evolution, we have come across a very interesting and intriguing phenomenon: the presence and nature of protic species switch "on" and "off" the change of morphology. In order to prove this statement, experiments aimed at revealing the dependence of the morphological evolution on different features of protic species were performed. For the sake of simplicity, the oxidizing action of molecular oxygen is considered to produce H_2O_2 in within the composition of the dispersive chloroformic medium by regarding alternatively the right side of eq. (1) or that of eq. (2):

$$\left[Ag_{(x)}\right]_{(NP)} + 2\,HSCN + O_2 + 2\left[CTA^+\cdots SCN^-\right] \rightarrow \ldots$$
$$\ldots \rightarrow \left[Ag_{(x-2)}\right]_{(NP)} + H_2O_2 + 2\left[CTA^+\cdots Ag(SCN)_2^-\right] \quad (3)$$

$$\left[Au_{(x)}\right]_{(NP)} + 2\,HBr + O_2 + 2\left[CTA^+\cdots Br^-\right] \rightarrow \ldots$$
$$\ldots \rightarrow \left[Au_{(x-2)}\right]_{(NP)} + H_2O_2 + 2\left[CTA^+\cdots AuBr_2^-\right] \quad (4)$$

where for eq. (4) it is assumed, by the sake of simplicity, that small AuNPs are oxidized to generate the dibromoaurite complex $AuBr_2^-$. From both equations follow that protic species (HSCN, HBr) are essential since they provide the ligand species (SCN^-, Br^-) which help the formation of complex anions ($Ag(SCN)_2^-$, $AuBr_2^-$) and the proton ions(H^+) for O_2 reduction to H_2O_2. These reactions were used as starting hypothesis to perform experiments for in assessing their consistency: if one of these reactions is somehow either altered or inhibited then a change in the rate of the morphological evolution should be detected.

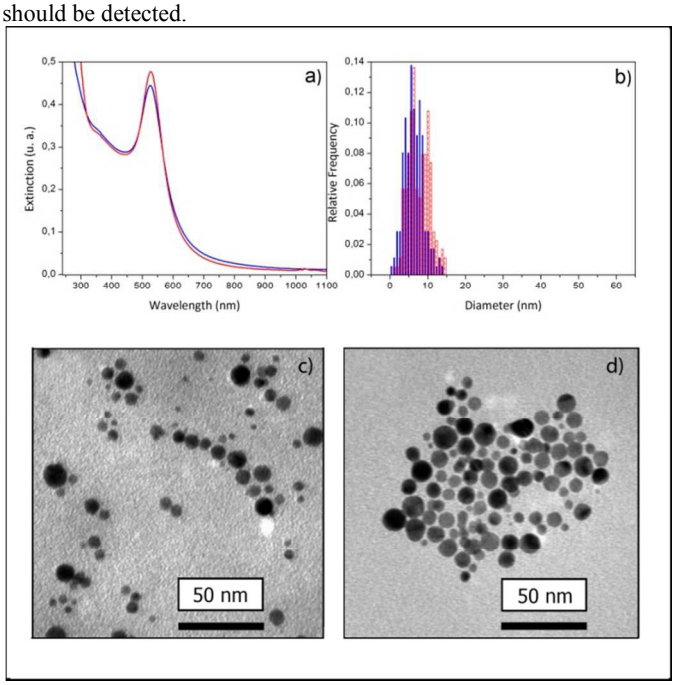

Figure 5. (a) UV-Vis spectral evolution of AuNPs in chloroform: (—) after formation and (—) at the 5th day of evolution in presence of triethylamine. (b) Size distribution of AuNPs: (—) after their formation ($\langle d\rangle = 6.1$ nm, $\sigma = 2.47$ nm) and (—) at the 5th day of evolution in presence of triethylamine ($\langle d\rangle = 7.4$ nm, $\sigma = 3.37$ nm). (c) TEM images of AgNPs produced with the reduction of $(CTA^+\cdots AuBr_4^-)$ with $(CTA^+\cdots BH_4^-)$ immediately after their formation ($\langle d\rangle = (6.1$ nm, $\sigma = 2.47$ nm) and (d) after five (5) days of evolution in presence of triethylamine ($\langle d\rangle = 7.4$ nm, $\sigma = 3.37$ nm).

Figure 5 shows the results obtained for AuNPs formed from $AuBr_4^-$ which were brought to evolve in presence of triethylamine over a period of five days. It can be clearly noticed that AuNPs' spectral profile after five days of evolution (Fig. 5.a, red line) retains the main features of the typical profile corresponding to freshly synthesized small AuNPs (Fig. 5.a, blue line), which were already described in Fig. 2. TEM micrographs of AuNPs evolved in presence of triethylamine at each stage show, at first glance, that morphology remains almost unchnged (Fig. 5c, 5d). A more detailed analysis reveals that AuNPs exhibit only a very slight increase of $\langle d\rangle$ from 6.1 nm to 7.4 nm and a small broadening of the size distribution (σ) from 2.47 nm to 3.37 nm. These very small changes of $\langle d\rangle$ and σ

obtained for morphological evolution of AuNPs in presence of triethylamine are quite contrasting with those already shown for AuNP evolution in absence of the amine (Fig. 2) within comparable evolution time. This behavior is indicative that triethylamine represents a very strong disturbance within the processes which determine the rate of the morphological evolution. This impressive result is consistent with the starting hypothesis of HBr working like a source of the proton ions (H^+) necessary for H_2O_2 formation and the ligand bromide anion (Br^-) needed to stabilize the oxidized Au(I) species ($AuBr_2^-$). Even though amines have been reported among stabilizing agents of AuNPs[39], triethylamine contribution as stabilizing agent cannot be evaluated because AuNPs in chloroform form already a perfectly stabilized dispersed phase even in absence of the amine molecule. According to the structure proposed for the electrostatic stabilization, it involves, firsly, the direct absorption of bromide ions on the surface of AuNPs[40], then, followed by the co-adsorption of the bulky tetraalkylammonium cations[24,32]. In this present work, the surfactants (trimethylhexadecylammonium salts) and solvent used allow to include also van der Waals interactions between the surfactant hydrocarbon chains[41] as an additional contribution to the stability of disperse system. The consideration of these experimental details allows in explaining reasonably the good stability observed.

Without any evidence indicating that triethylamine produces some improvement in the stabilization of AuNPs, triethylamine influence is analyzed by considering its Lewis base properties. Given the AuNPs evolution is greatly quenched in presence of triethylamine, then it is reasonable in considering that an acid-base process takes place, according to:

$$(Et)_3N + HBr \rightarrow \left[\{(Et)_3NH\}^+\cdots Br^-\right] \quad or \quad \left[(Et)_3N\cdots H\cdots Br\right] \qquad (5)$$

Where, at the right side of eq. (5), the hypothetic species correspond to the possible products whether if the reaction involves a net proton transference to produce an ionic pair or if the formation of a chemical bond to produce an adduct compound is the process taking place. Whatever the nature of the product obtained from the reaction (5), there is a clear fact there: Lewis base properties of triethylamine introduce a strong disturbance in the sequence of steps **C-D-RD**. The change of reactivity associated with a noticeably less dynamic AuNPs morphological evolution can be understood by realizing that reaction (5) represents for the reduction of O_2 to H_2O_2 (step **C**) a process which competes for proton ions (H^+). Triethylamine helps in revealing that HBr, a protic species with a highly polar hydrogen bond and an anion with strong ligand properties (Br^-), plays a central role in the dynamics of the morphological evolution of AuNPs. Another interesting way of testing the role of protic species is, however, by studying the morphological stability of NPs in presence of protic species with less polar hydrogen bond or only able of producing anions with poor ligand properties. Since the protic species are produced during the NP formation, the synthesis has to be made by using a different precursor agent order to change the chemical identity of the protic species.

Figure 6 shows the spectral curves obtained from the synthesis of AgNPs based on the reduction of Ag_2O driven by BH_4^- in chloroformic environment. A colloidal suspension is obtained from the mixing of the powdered Ag_2O with chloroform, where probably only a small fraction of Ag_2O is in the form of soluble species. The chloroformic colloidal Ag_2O exhibits a spectral profile with an almost constant extinction along the whole visible range (Fig. 6a, black line). After the addition of BH_4^-, the spectral profile of the reactive solution presents an SPR peak at 415 nm, associated with the AgNP formation (Fig. 6a, red line) (ESI-Fig. 3). The reaction continues and, during a couple of days, the extinction peak of AgNP SPR increases noticeably its intensity and the profile becomes wider (Fig. 6a, green and blue lines). The chloroformic reactive solution was filtered to separate Ag_2O particles that might have not reacted and different aliquots were used to perform different essays.

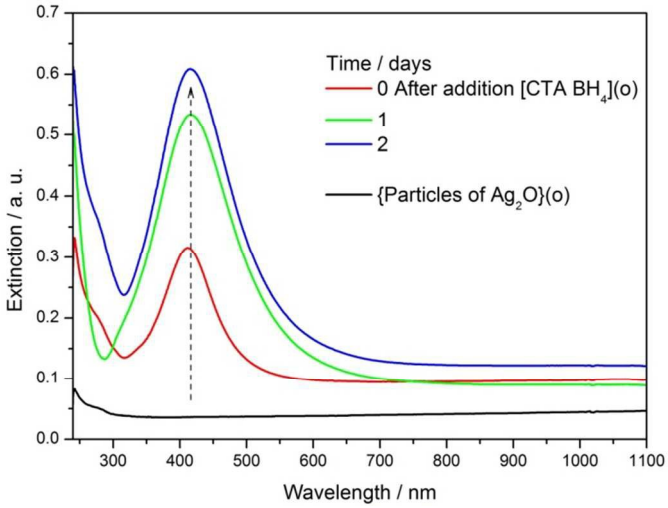

Figure 6. Formation of AgNPs from reduction of chloroformic Ag_2O colloid with borohydride of trimethyl-hexadecil-ammonium ($CTA^+\cdots BH_4^-$) liquor. UV-Visible spectra corresponding to: (—) the initial Ag_2O particles chloroformic suspension and (—, —, —) the evolution after the addition of BH_4^-.

The supernatant exhibits a spectral evolution where the extinction peak of the AgNP SPR increases as time elapses. The changes in the spectrum profile, however, become more subtle at longer reaction time (ESI-Fig. 4). Such a trend is a clear indication that the formation reaction continues, driving nucleation and growth of AgNPs. This evolution of the spectral profile suggests clearly that no morphological evolution is taking place despite that protic species are formed as by-products from the BH_4^- oxidation. Here, it is relevant to consider the polar character of the hydrogen bond of the protic species produced by the AgNP formation reaction. Evidently, Ag_2O is a source of oxide anions (O^{2-}) that broadens the possible oxidation processes of BH_4^-. It is also important to notice, however, that the principle of electroneutrality of the matter must be also fulfilled. Accordingly, hypothetical processes like the following can be written:

$$2\,Ag_2O_{(s)} + \left[CTA^+\cdots BH_4^-\right] \rightarrow 4\,Ag_{(NP)} + H_2O + \left[CTA^+\cdots H_2BO^-\right] \qquad (6)$$

It can be seen that the protic species proposed as by-product in eq. (6), H_2O; has a hydrogen bond which is clearly less polar than that of HSCN, just like their relative water acidity values indicate. However, aside from this discussion, the fact of having found this chloroformic AgNPs dispersion which owns a remarkable morphological stability does offer an opportunity: the main hypothesis can be assessed experimentally by the addition of a protic species with a very well known chemical behavior into this morphologically stable dispersion in order to "switch on" the *pseudo*-Ostwald ripening stage of AgNPs (Fig. 7). The addition of benzoic acid into this chloroformic AgNPs disperse system triggers a noticeable decrease of the characteristic SPR peak during the first couple of hours. As the reaction time elapses, the slight extinction increase for wavelength values higher than 550 nm is associated with the size increase of a fraction of NPs within the whole population. This spectral evolution for long time values is clearly indicative

that changes in size of AgNPs are taking place. Thus, the key sequence of steps **C-D-RD** is again "switched on" after the addition of benzoic acid, corroborating that protic species are playing a central role in the morphological evolution of AgNPs.

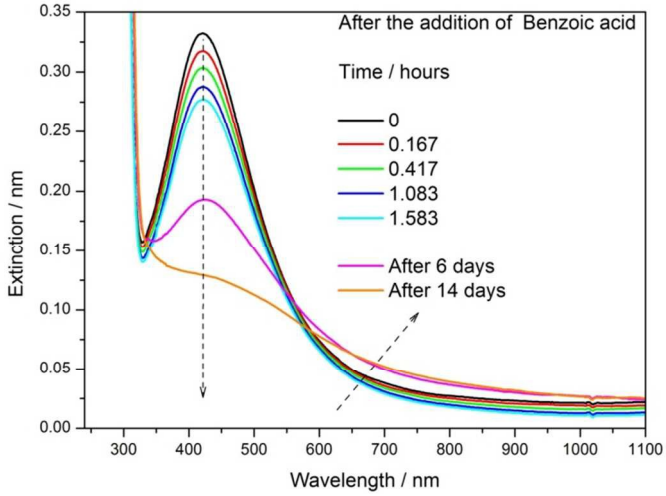

Figure 7**.** Evolution of AgNPs in presence of benzoic acid. UV-Visible spectra of the evolution of AgNPs in chloroform after the addition of benzoic acid.

The achievement of a consistent description of *pseudo*-Ostwald ripening of AuNPs and AgNPs in chloroform in terms of an electrhochemical mechanism is a result worthy of being highlighted. In addition, it is unavoidable to remark the close resemblance of the mechanism proposed in the present study and that unraveled in the pioneering work of Brus' team[19]: both mechanisms are of electrochemical nature. If this likeness seems a promising clue, the unlikeness between them suggests a more general portrait. Indeed, the fact that the electrochemical mechanism provides a suitable description of the Ostwald ripening of nanoparticles immersed in either chloroform or water[19], and independently of that it be nanoparticles in colloidal suspension or onto conductive/insulator substrates[19] does suggest the validity of this electrochemical mechanism is general.

Conclusions

The morphological stability / morphological reshaping evolution of noble metal nanoparticles in chloroform was studied by means of model synthetic systems. Starting from reactive species spectroscopically characterized, overall reactions for the NP formation were proposed and used for posing hypothetical composition of the chloroformic medium where morphological evolution NPs takes place. The increase of NP average size and the broadening of its size distribution which are the main features of the morphological evolution can be explained in terms of a *pseudo*-Ostwald ripening stage which involves steps of corrosion, diffusion of intermediary species and a re-deposition. NP corrosion is driven by the molecular oxygen dissolved in the dispersive medium only if protic species participate as co-reactive. These key protic species do enable the morphological evolution of NPs when they owns a highly polar hydrogen bond and are able of producing ligand anions to form complexes with the oxidized species generated from NPs. Protic species without these main features deactivate the corrosion step, disabling the morpological evolution.

Acknowledgements

We thank Claudia Nome from IPAVE for her technical assistance in TEM, to Mathias Douglas Gallardo for his advice in graphic design, and to Martin Harvey for his proof reading. Oscar A. Douglas-Gallardo thanks Consejo Nacional de Investigaciones Científicas y Técnicas (CONICET) for his fellowship. We'd especially like to thank Dr. Miguel Jose Yacaman for his selfless assistance in part of this work. In Argentina, this proyect has been supported by the CONICET, the Fondo para la Investigación Científica y Tecnológica (FONCyT) of Argentina, Agencia Nacional de Promoción Científica y Tecnológica (ANPCyT) Program BID, and the Secretaría de Ciencia y Tecnología (SECYT- UNC) by means of different grants (PME(2006) 1544, PIP (2012) 112-201101-00430, PIP (2012) 112-200801-000983, PICT (2012) 2286, PICT (2010) 1233). In EE.UU., this project was supported by a grant from the National Institute on Minority Health and Health Disparities (G12MD007591) from the National Institutes of Health (NIH).

Notes and references

[a] *INFIQC - Departamento de Fisicoquímica, Facultad de Ciencias Químicas, Universidad Nacional de Córdoba, Ciudad Universitaria. Pabellón Argentina, Ala 1, 2do piso, Haya de la Torre. 5000 Córdoba, Argentina. Fax: +54 351 4334188; Tel: +54 351 4334180;*
e-mail: mperez@fcq.unc.edu.ar
[b] *Departamento de Química Orgánica, Facultad de Ciencias Químicas, Universidad Nacional de Córdoba, Ciudad Universitaria. Edificio de Ciencias II, Haya de la Torre y Medina Allende, 5000 Córdoba, Argentina.*

.

† Electronic Supplementary Information (ESI) available: A) STEM and EDS of AgNPs (ESI-Fig. 1) and AuNPs (ESI-Fig. 2). B) TEM of AgNPs produced from of Ag_2O colloids (ESI-Fig. 3). C) Spectral behaviour of AgNPs produced from of Ag_2O colloids during the formation stage (ESI-Fig. 4).

1 C.N.R. Rao, G.U. Kulkarni, P.J. Thomas, P.P. Thomas, *Chem. Soc. Rev.*, 2000, **29**, 27-35.
2 C.N.R. Rao, G.U. Kulkarni, J. P. Thomas, P.P. Edwards, *Chem. Eur. J.* 2002, **8**, 29-35
3 M.C. Daniel, D. Astruc, *Chem. Rev*. 2004, **104**, 293-3461.
4 J.A. Blackman, C. Binns, Ch. 1 in "Metallic Nanoparticles" from the series "Handbook of Metal Physics", John Blackman Ed., Elsevier, Amsterdam, 2009.
5 F. Le, D.W. Brandl, Y.A. Urzhumov, H. Wang, J. Kundu, N.J. Halas, J. Aizpurua, P. Nordlander, *ACS Nano* 2008, **2**, 707-718.
6 C.J. Murphy, A.M. Gole, S.E. Hunyadi, C.J. Orendorff, *Inorg. Chem.* 2006, **45**, 7544-7554.
7 M.A. Pérez, Chap. 6: "Growth Mechanisms of Metal Nanoparticles", p.143-160, In Recent advances in Nanoscience, M. M. Mariscal and S. A. Dassie Eds. Research Signpost, Kerala, India, 2007.
8 M. Brust, M. Walker, D. Bethell, D.J. Schiffrin, R. Whyman, *J. Chem. Soc., Chem. Commun.*1994, 801-802.
9 J. Yang, J. Yang Lee, T.C. Deivaraj, H-P. Too, *Colloids Surf., A: Physicochemical and Eng.* 2004, **240**, 131-134.
10 P.J.G. Goulet, R.B. Lennox, *J. Am. Chem. Soc.* 2010, **132**, 9582-9584.

11 Y. Li, O. Zaluzhna, B. Xu, Y. Gao, J.M. Modest, Y.J. Tong, *J. Am. Chem. Soc.* 2011, **133**, 2092-2095.
12 Y. Li, O. Zaluzhna, Y.J. Tong, *Langmuir* 2011, **27**, 7366-7370.
13 Y. Li, O. Zaluzhna, C.D. Zangmeister, T.C. Allison, Y.J. Tong, *J. Am. Chem. Soc.* 2012, **134**, 1990-1992.
14 G. Corthey, A.A. Rubert, A.L. Picone, G. Casillas, L.J. Giovanetti, J.M. Ramallo-López, E. Zelaya, G.A. Benitez, F.G. Requejo, M.J. Yacamán, R.C. Salvarezza, M.H. Fonticelli, *J. Phys. Chem. C.* 2012, **116**, 9830-9837.
15 M.M. Oliveira, D. Ugarte, D. Zanchet, A.J.G. Zarbin, *J. Colloid Interface Sci.* 2005, **292**, 429.
16 K. Meguro, M. Torizuka, K. Esumi. *Bull. Chem. Soc. Jpn*. 1988, **61**, 341.
17 K. Meguro, T. Tano, K. Torigoe, H. Nakamura, K. Esumi. *Colloids surf.*1988/1989, **34**, 381.
18 H. Bönnemann, R. Brinkmann, R. Köppler, P. Neiteler, J. J. Richter. *Adv. Mater*. 1992, 4, 804.
19 P. L. Redmond, A. J. Hallock, L. E. Brus, *Nano Lett.* 2005, **5**, 131-135.
20 A. Schröder , J. Fleig , D. Gryaznov, J. Maier , W. Sitte, *J. Phys. Chem. B* 2006, **110**, 12274–12280
21 P. Parthasarathy, A. V. Virkar, *J. Power Sources* 2013, **234**, 82-90.
22 C. J. D. von Grotthuss, *Ann. Chim.* 1806, **58**, 54-73.
23 N. Agmon, *Chem. Phys. Lett.* 1995, **244**, 456-462.
24 H. Bönnemann, W. Brijoux, R. Brinkmann, E. Dinjus, T. Joußen, B. Korall. *Angew. Chem. Int. Ed. Engl*. 1991, *30*, 1312.
25 R.A. Jones, *"Quaternary Ammonium Salts - Their Use in Phase-Transfer Catalysis (Best Synthetic Methods)"*, Academic Press, Kent, 2001.
26 M. Cox, J. Rydberg; Y. Marcus; G.R. Choppin; J. Rydberg, G.R. Choppin, C. Musikas and T. Sekine; P.R. Danesi; Ch. 1-5 in *"Solvent Extraction - Principles and Praciice"*, J. Rydberg, M. Cox, C. Musikas, G.R. Choppin Eds., Marcel Dekker Inc.,New York, 2004.
27 L. V. Titov, L. A. Gavrilova, E. R. Eremin, S. S. Mishchenchuk, V. Ya. Rosolovskii. *Russ. Chem. Bull*. 1971, 20, 1266-1268.
28 L. Klicova, P. Sebej, P. Stacko, S. K. Filippov, A. Bogmolova, M. Padilla, P. Klan. *Langmuir*. 2012, **28**, 15185-15192.
29 A. Usher, D. C. McPhail, J. A. Brugger. *Geochim. Cosmoquim. Acta*. **73**, 2009, 3359-3380.
30 K. Nakamoto, *Infrared and Raman Spectra of Inorganic and Coordination Compounds*, 4th Ed., John Wiley & Sons, New York, 1987.
31 H. Stammreich, R. Forneris. *Spectrochim. Acta*. **16**, 1959, 363-367.
32 I. E. Molinou, N. G. Tsierkezos. *Spectrochim. Acta A*. 2008, **71**, 954–958.
33 P.J. Larkin, IR and Raman Spectroscopy: Principles and spectral interpetration, Elsevier, San Diego, 2011.
34 T. Mortier, A. Persoons, T. Verbiest. *Inorg. Chem. Commun.* 2005, **8**,1075-1077.
35 P. J. G. Goulet, A. Leonardi, R. B. Lennox. *J. Phys. Chem.* 2012, **116**, 14096-14102.
36 G. Zotti, B. Vercelli. *Anal. Chem*. 2008, **80**, 815-818.
37 M. Dasog, R. W. J. Scott. *Langmuir*. 2007, **23**, 3381-3387.
38 C-K Tsung, X. Kou, Q. Shi, J. Zhang, M. H. Yeung, J. Wang, G. D. Stucky. *J. Am. Chem. Soc*. 2006, 128, 5352-5353.
39 K. G. Thomas, J. Zajicek, P. V. Kamat. *Langmuir*. 2002, **18**, 3722-3727.
40 Z. Dengt, D. E. Irish; *J. Phys. Chem.* 1994, **98**, 11169-11177.
41 S. Praharaj, S. K. Ghosh, S. Nath, S. Kundu, S. Panigrahi, S. Basu, T. Pal, *J. Phys. Chem. B* 2005, **109**, 13166-13174.

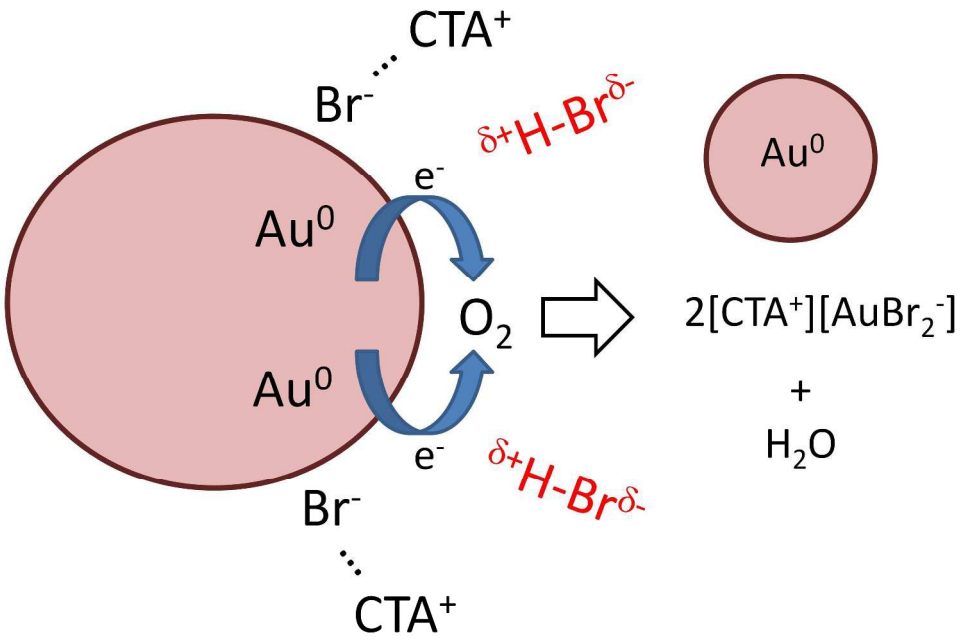

945x668mm (96 x 96 DPI)